RSC Advances

ROYAL SOCIETY OF CHEMISTRY

www.rsc.org/advances

Strong ferromagnetism beyond the mechanism of uncompensated surface spins in nanocrystalline $GaCMn_3$

B. Song,†[a,b] J. C. Lin,†[a] P. Tong,*[a] M. Wang,[a] C. Yang,[a] X. G. Guo,[a] S. Lin,[a] and Y. P. Sun*[acd]

[a] *Key Laboratory of Materials Physics, Institute of Solid State Physics, Chinese Academy of Sciences, Hefei 230031, People's Republic of China*

[b] *School of Physics and Materials Science, Anhui University, Hefei 230601, People's Republic of China*

[c] *High Magnetic Field Laboratory, Chinese Academy of Sciences, Hefei 230031, People's Republic of China*

[d] *Collaborative Innovation Center of Advanced Microstructures, Nanjing University, Nanjing 210093, People's Republic of China*

Abstract

Weak ferromagnetism arising from uncompensated surface spins (USS) is usually expected when an antiferromagnetic (AFM) material is diminished to nanoscale in size. Here we reported strong ferromagnetism beyond the USS-mechanism in the AFM ground state of nanocrystalline $GaCMn_3$. The enhanced ferromagnetism can be attributed to a AFM to ferromagnetic (FM) transformation in the shell with finite thickness of a crystallite. As the average crystallite size (<*D*>) decreases, the FM shell expands relative to the AFM core, leading to the strengthening ferromagnetism. Through the AFM/FM interface the rotation of FM spins under a magnetic field is impeded by the AFM spins, leading to a large coercivity (H_C). The largest H_C (~ 6.4 kOe at 5 K) was observed in the sample with critical <*D*> of ~ 15 nm. In contrast, USS-type weak ferromagnetism was observed in nanocystalline $GaNMn_3$. Our results suggest a new approach to achieving strong FM order beyond the prediction of the USS mechanism, as well as to designing AFM-core/FM-shell nanostructure based on nanosized AFM materials.

a) E-mail: tongpeng@issp.ac.cn

b) E-mail: ypsun@issp.ac.cn

† These authors contributed equally to this work and should be considered as cofirst authors.

1. Introduction

Nanocrystallline magnetic materials usually ranging in dimension from 1 to 100 nanometers (*nm*) have properties unique from their bulk equivalent, which have great potential applications.[1,2] In turn, the related properties can be effectively tailored by reducing the crystallite size, particularly to nanoscale.[1-4] For small nanoparticles of an antiferromagnetic (AFM) material, the surface spins are expected to dominate the measured magnetization because of their lower coordination and uncompensated exchange couplings.[2, 5] In nanosized oxides, such as MnO,[6, 7] NiO,[7, 8] CuO,[9] Cr_2O_3,[10] and $CoRh_2O_4$,[11] the weak ferromagnetism has been widely observed and the mechanism of uncompensated surface spins (USS) was often quoted to explain their magnetic behaviors.

Manganese-based antiperovskite compounds $AXMn_3$ (A: metal or semiconducting elements, X: C or N) adopt a simple cubic crystal structure (space group, *Pm-3m*).[12] In the cubic lattice, element A locates at the corner positions, X at the body center, and Mn at the face centers. Although structurally analogous to their perovskite oxides counterparts (i.e., manganites), $AXMn_3$ compounds exhibit good electric and thermal conductivities.[13] Moreover, new functionalities were continuously reported, including giant barocaloric effect,[14] large magnetocaloric effect,[15-17] negative or zero thermal expansion,[18-22] giant magnetoresistance,[23-25] nearly zero temperature coefficient of resistance,[26-28] and giant magnetostriction.[29] Recently, nanocrystalline antiperovskite $Cu_{1-x}Ge_xNMn_3$ (x = 0.4 and 0.5) and $Zn_{0.6}Ge_{0.4}NMn_3$ were reported to have wider temperature spans of negative thermal expansion than their micro-crystallite counterparts.[19, 21] Competing ferromagnetic (FM) order was introduced to the AFM ground state and suggested to delays the growth of the AFM order upon cooling which is closely related to the lattice

expansion.[19, 21] Otherwise, the underlying physics of the introduced FM order and evolution of magnetic properties with reducing crystallite size haven't been addressed for antiperovskite compounds.

Here we report a comparison study of the magnetic properties of nanocrystalline $GaCMn_3$ and $GaNMn_3$ prepared by high-energy ball milling. Despite the fact that both compounds exhibit AFM ground states in bulk samples, the magnetic properties of nanocrystalline samples are distinct. Nanocrystalline $GaNMn_3$ shows weak ferromagnetism as expected by the USS mechanism. However, enhanced magnetization along with large magnetic coercive field up to 6.4 kOe was observed in nanocrystalline $GaCMn_3$. A stiff FM shell against the AFM core was suggested to form as a result of AFM-FM transition caused by the boundary/surface stress, which differs essentially from the USS scenario. The AFM-core/FM-shell model explains the large coercivity and how it changes with temperature and crystallite size.

2. Experimental details

Polycrystalline samples of $GaCMn_3$ were prepared directly by the solid-state reaction from commercially available Ga ingot (4N), Graphite (3N) and Mn (4N) powders.[22] The as-prepared sample was crushed into powders and then sealed with zirconia balls and alcohol (as wet medium) in a stainless steel vial in Ar atmosphere. The ball to powder to alcohol weight ratio was 8:1:0.6. The milling process was carried out at a constant speed (200 rpm) using a high-energy planetary ball mill (QM-IF). The milling time varies from 5 hours to 40 hours. The preparation and characterizations of nanocrystalline $GaNMn_3$ were reported in Ref 22. X-ray diffractions (XRD) for all samples were measured using a Bruker D8 discover X-ray diffractometer with Cu K_α radiation (λ= 0.15406 *nm*) at room temperature. The surface morphology was measured using a field-emission scanning electronic microscope (FE-SEM, FEI-designed Sirion 200, Hillsboro, OR). The magnetic measurements were performed on a Quantum Design Superconducting Quantum Interference Device (QD-SQUID) magnetometer (1.8 K $\leq T \leq$ 400 K, 0 $\leq H \leq$ 50 kOe).

3. Results and discussion

Figure 1 shows the powder X-ray diffraction patterns at room temperature for the $GaCMn_3$ samples with milling of 0 hour (BM-0h, i.e., the as-prepared sample) to 40 hours (BM-40h). Bragg reflections for each sample can be well indexed with the cubic antiperovskite structure (space group, *Pm-3m*). The X-ray diffraction peaks become broader as the milling time increases, which can be primarily attributed to the reduced crystallite size.[21] For nanocrystalline materials, the crystallite size (<*D*>) can be calculated using X-ray diffraction peaks by means of the well-known Scherrer formula: $<D> = 0.93\lambda/(B\cos\theta)$,[30] where λ is the wavelength of the X-ray radiation, θ the diffraction angle position of the peaks, and *B* is the full width at half-maximum of the peak after taking into account the instrumental peak broadening. The value of <*D*> was estimated seperately using (111), (200), (111) and (220) diffraction peaks. Then the average <*D*> was then obtained based on the four calculated values. The average <*D*> for the BM-0h sample is about 845 *nm*, which may not be reliable because the Scherrer method only works when the crystallite size in a sample of interest lies in the range between 5 nm and 50 nm.[30] As the milling time increases, the crystallite is minished to 45 *nm*, 28 *nm*, 15 *nm*, 12 *nm* and 9 *nm* for BM-5h, BM-10h, BM-20h, BM-30h and BM-40h samples, respectively. The refined lattice constant (a_0) is decreased after milling, as shown in the inset of Fig.1. Upon ball milling, the particle size is reduced as expected (Fig. 2(a)-(c)). Most particles are larger than 5 μm for slightly crushed bulk sample (Fig. 2(a)), while for BM-40h sample the largest particle is only 2-3 μm in size.

Figure 3(a) shows the temperature dependent magnetization *M*(T) for $GaCMn_3$ samples measured under zero-field-cooling mode with a magnetic field of 100 Oe. For the bulk sample, the three characteristic transitions are clearly seen, namely a FM to paramagnetic (PM) (FM-PM) transition at $T_C \sim 246$ K, an intermediate (IM) to FM (IM-FM) transition at $T_I \sim 180$ K, and then an AFM-IM transition at $T_N \sim 165$ K. These characteristic temperatures are close to those reported previously.[31] The distinguishable T_N and T_I indicate a good quality of our sample. Based on the

differential M(T), dM(T)/dT in Fig. 3(b), the transition temperatures for other samples were determined and plotted in Fig. 3(c) as a function of crystallite size. In the initial stage of milling, T_N decreases dramatically when <D> is reduced to 45 *nm*, while T_C is little affected. T_N is nearly invariable with further reducing <D> to 15 *nm*, at which T_C takes a jump. When <D> is less than 15 *nm*, T_C keeps nearly as a constant, but the abnormality at T_N on the dM(T)/dT curve is smeaed out.

Figure 4(a) shows the field scanning of magnetization, M(H), at 5 K for all $GaCMn_3$ samples. M(H) for the non-milled bulk sample is small in magnitude. It exhibits a linear field dependence with a zero coercive field (H_C). This coincides with the AFM ground state of the micro-crystallite $GaCMn_3$.[31] As <D> decreases, the M(H) loop becomes wide and H_C increases. Simutaneously, the magnetization at 45 kOe (M_{45kOe}) is increased notably. The magnetization is quite large and comparable to that measured at the FM state of micro-crystallite $GaCMn_3$.[32] The large magnetization and high H_C indicate a FM order was introduced below T_N in nanocrystalline $GaCMn_3$. As shown in Fig. 4(b), H_C increases initially with reducing <D> down to 15 *nm*, and then decreases as <D> reduces further. When <D> is larger than 15 *nm*, M_{45kOe} reduces gradually as <D> increases. However, M_{45kOe} is enhanced sharply as <D> is reduced to be smaller than 15 *nm*. H_C at 5 K is 6.4 kOe for the sample with critical crystallite size, <D> = 15 *nm*. Temperature dependent M(H)s were measured for the sample with <D> = 15 *nm* and displayed in Fig. 5(a). As shown in Fig. 5(b), M_{45kOe}(T) peaks at 150 K which basically coincides with the AFM transition at T_N ~ 165 K estimated from the M(T) data. Accordingly, H_C decreases gradually as the sample is heated up to 150 K. When being heated well above T_N, e.g., at 230 K, H_C drops nearly to zero. The crystallite size and temperature dependences of H_C and M_{45kOe} strongly suggest that the magnetic coercivity of the FM order is closely related to the coexisting AFM order.

For a ferromagnet its direction of magnetization can be reversed either continuously through rotation process or discontinuously through domain process.[33] As shown in Fig. 4(a) and Fig. 5(a), the initial process of magnetization under magnetic field is quite slow, which suggests a

rotation process rather than a domain process.[33] Crystallographic anisotropy is the most effective means of impeding magnetization reversal by rotation process.[33] However, for antiperovskite compounds this effect should be very weak because of the isotropic crystal structure. Alternatively, a coexisting AFM component with small anisotropy can cause an enhanced H_C. In this case, when the FM spins rotate it drags the AFM spins irreversibly through the AFM/FM interface, hence yielding large FM coercivity.[34, 35]

As a comparison, the magnetic properties of ball-milled $GaNMn_3$ were measured and plotted in Fig 6. As shown in Fig. 6(a), the bulk $GaNMn_3$ exhibits a AFM-PM transition at $T_N \sim 318$ K. As the crystallite is diminished, the transition is shifted to lower temperatures (Fig. 6(b) and (c)), which accords well with our previous results of Differential Scanning Calorimeter (DSC) and temperature dependent X-ray powder diffractions.[22] Finally, T_N is reduced to 285 K as the crystallite size is decreased to 13 *nm*. Fig. 6(d) displays the M(H) at 5 K for $GaNMn_3$ samples with various values of crystallite size. It is clear that weak ferromagnetism was introduced in addition to the AFM state in the sample with $\langle D \rangle = 13$ *nm* as evidenced by the weak coercivity (0.59 kOe) and slightly increased magnetization. However, M(H) still shows a linear H dependence for $H > 10$ kOe with a large slope. Moreover, the magnitude of M(H) is quite small even at 45 kOe (~ 3 emu/g). Therefore, the observed weak ferromagnetism can be attributed to the uncompensated spins at crystallite/grain surfaces, as has been often argued for other nanosized AFM materials.[6-11] On the contrary, the ferromagnetism (e.g., $M_{45kOe} = 42$ emu/g at 5 K for $\langle D \rangle = 9$ *nm*) observed in nanocrystalline $GaCMn_3$ is stronger than those of most USS-oxides.[6-9, 11] Moreover, for USS-ferromagnetism, the magnetization usually increases with increasing temperature due to a thermal-induced contribution to the magnetism.[5] In our case, however, a dome-like temperature dependence of M_{45kOe} was observed for $GaCMn_3$ with $\langle D \rangle = 15$ *nm.* Consequently, the strong magnetization and it temperature dependence indicate the FM order in nanocrystalline $GaCMn_3$ cannot be comprehended in the framework of USS.

As shown in the inset of Fig. 1, the overall lattice tends to shrink after milling. This is fairly

normal for nanocrystalline materials because the interface/grain boundary stress can add a hydrostatic pressure on the lattice and leads to a volume contraction as the crystallite size reduces.[36] The core of a crystallite should be less affected than the shell since the AFM order is retained to some extent. As a consequence, the stress should be spatially inhomogeneous, i.e., it decays with distance from the surface to the core of a crystallite. As revealed by high pressure experiment, a smaller lattice favors FM coupling rather than AFM coupling in $GaCMn_3$ and thus a pressure-trigered AFM-FM transition was observed.[37] Therefore, a FM shell with finite thickness may form against the AFM core in the nanosized crystallites. Such a AFM-FM transfomation leads to enhancement of magnetism as shown in Fig. 4. Consistently, the reduced T_N and enhanced T_C in nanocrystalline $GaCMn_3$ relative to the bulk one resembles the result of high pressure experiment.[37] The lattice of $GaNMn_3$ also shrinks as $<D>$ decreases,[22] which shifted T_N to lower temperature as high pressure did.[14] However, the AFM ground state is rigid against the high pressure.[14] So, one can not anticipate a AFM-FM transition due to stress effect at the surface of nanosized crystallites. Therefore, the weak ferromagnetism observed in nanocrystalline $GaNMn_3$ can be reasonably attributed to the USS senario. The surface/surface-stress induced FM shell against the AFM core may provide an alternative approach to constructing a AFM-core/FM-shell nanostructure based on AFM magnetials, in which large coercivity and even exchange bias can be expected.[35]

The aforementioned AFM-core/FM-shell structure provides a physical background for the evolutions of H_C and M_{45kOe} with $<D>$ and temperature plotted in Figs. 4(b) and 5(b). As $<D>$ decreases, the large crystallites split. Thus, the overall surface-to-volume ratio increases, increasing the AFM/FM interfaces and thus resulting in an increase of H_C. Simultaneously, as the milling time increases the FM shell will become thicker at the expense of the AFM core, which will decrease the AFM/FM interface and accordingly reduce H_C. As a combination of the above two effects, H_C increases initially with reducing $<D>$ down to a critical value (i.e., 15 *nm*) and then decreases upon further reducing $<D>$. As $<D>$ is fixed at the critical value, H_C is determined

by the strength of the AFM order. As temperature rises from 5 K to 150 K which is very close to T_N, the AFM coupling is increasingly weakened owing to the enhanced thermal fluctuations. As a result, H_C reduces gradually as temperature increases to 150 K. At temperatures well above T_N, the AFM couplings are random and thus does not hinder the FM rotation, leading to a nearly zero H_C as shown in Fig. 5(b). In addition, as the crystallite size reduces the thickness of the FM shell increases relative to the AFM core, leading to the increasingly strenghthened ferromagnetism (Fig. 4).

IV. CONCLUSION

In summary, we compared the magnetic properties of nanocrystalline $GaCMn_3$ and $GaNMn_3$ prepared by mechanically grinding. Unlike the weak ferromagnetism observed in nanocrystalline $GaNMn_3$, strong magnetization together with large H_C up to 6.4 kOe found in nanocrystalline $GaCMn_3$ suggests a different mechanism from the well-known USS model. We proposed that in nanocrystalline $GaCMn_3$ a FM surface shell is formed against the AFM core due to a stress-induced AFM-FM transition. The competition between the FM-shell and AFM-core and the interface between them explain the evolutions of H_C with crystallite size and temperature. Our current results may open a new avenue for designing AFM-core/FM-shell structure at nanoscale, which is a fundamental configuration for achieving large H_C and/or exchange bias in nanostructured systems.

Acknowledgments

The authors acknowledge the financial support from the National Key Basic Research under Contract Nos. 2011CBA00111 and the National Natural Science Foundation of China under Contract nos. 51322105, 11174295, 51301167, 51171177, 91222109.

References

1 M. E. McHenry and D. E. Laughlin, *Acta Mater.*, 2000, **48**, 223-238.

2 S. Mørup, D. E. Madsen, C. Frandsen, C. R. H. Bahl and M. F. Hansen, *J. Phys.: Condens. Matter*, 2007, **19**, 213202.

3 X. G. Zheng, H. Kubozono, H. Yamada, K. Kato, Y. Ishiwata and C. N. Xu, *Nat. Nanotechnol.*, 2008, **3**, 724-726.

4 R. F. Wang, C. Nisoli, R. S. Freitas, J. Li, W. McConville, B. J. Cooley, M. S. Lund, N. Samarth, C. Leighton, V. H. Crespi and P. Schiffer, *Nature*, 2006, **439**, 303-306.

5 S. Mørup and C. Frandsen, *Phys. Rev. Lett.*, 2004, **92**, 217201.

6 G. H. Lee, S. H. Huh, J. W. Jeong, B. J. Choi, S. H. Kim and H. C. Ri, *J. Am. Chem. Soc.*, 2002, **124**, 12094-12095.

7 M. Ghosh, K. Biswas, A. Sundaresan and C. N. R. Rao, *J. Mater. Chem.*, 2006, **16**, 106-111.

8 M. P. Proenca, C. T. Sousa, A. M. Pereira, P. B. Tavares, J. Ventura, M. Vazquez and J. P. Araujo, *Phys. Chem. Chem. Phys.*, 2011, **13**, 9561-9567.

9 A. Punnoose, H. Magnone, M. S. Seehra and J. Bonevich, *Phys. Rev. B*, 2001, **64**, 174420.

10 D. Tobia, E. Winkler, R. D. Zysler, M. Granada and H. E. Troiani, *Phys. Rev. B*, 2008, **78**, 104412.

11 R. N. Bhowmik, R. Nagarajan and R. Ranganathan, *Phys. Rev. B*, 2004, **69**, 054430.

12 K. Takenaka, M. Ichigo, T. Hamada, A. Ozawa, T. Shibayama, T. Inagaki and K. Asano, *Sci. Technol. Adv. Mater.*, 2014, **15**, 015009.

13 P. Tong, B. S. Wang and Y. P. Sun, *Chin. Phys. B*, 2013, **22**, 067501.

14 D. Matsunami, A. Fujita, K. Takenaka and M. Kano, *Nat. Mater.*, 2015, **14**, 73-78.

15 J. Yan, Y. Sun, H. Wu, Q. Z. Huang, C. Wang, Z. X. Shi, S. H. Deng, K. W. Shi, H. Q. Lu and L. H. Chu, *Acta Mater.*, 2014, **74**, 58-65.

16 O. Çakır and M. Acet, *Appl. Phys. Lett.*, 2012, **100**, 202404.

17 B. S. Wang, P. Tong, Y. P. Sun, X. Luo, X. B. Zhu, G. Li, X. D. Zhu, S. B. Zhang, Z. R. Yang, W. H. Song and J. M. Dai, *Europhys.Lett.,* 2009, **85**, 47004.

18 K. Takenaka and H. Takagi, *Appl. Phys. Lett.*, 2005, **87**, 261902.

19 X. Y. Song, Z. H. Sun, Q. Z. Huang, M. Rettenmayr, X. M. Liu, M. Seyring, G. N. Li, G. H. Rao and F. X. Yin, *Adv. Mater.*, 2011, **23**, 4690.

20 C. Wang, L. H. Chu, Q. R. Yao, Y. Sun, M. M. Wu, L. Ding, J. Yan, Y. Y. Na, W. H. Tang, G. N. Li, Q. Z. Huang and J. Lynn, *Phys. Rev. B*, 2012, **85**, 220103.

21 J. Tan, R. J. Huang, W. Wang, W. Li, Y. Q. Zhao, S. P. Li, Y. M. Han, C. J. Huang and L. F. Li, *Nano Res.,* 2015, **8**, 2302–2307.

22 J. C. Lin, P. Tong, X. J. Zhou, H. Lin, Y. W. Ding, Y. X. Bai, L. Chen, X. G. Guo, C. Yang, B. Song, Y. Wu, S. Lin, W. H. Song, and Y. P. Sun, *Appl. Phys. Lett.*, 2015, **107**, 016540.

23 K. Kamishima, T. Goto, H. Nakagawa, N. Miura, M. Ohashi, N. Mori, T. Sasaki and T. Kanomata, *Phys. Rev. B*, 2000, **63**, 024426.

24 Y. B. Li, W. F. Li, W. J. Feng, Y. Q. Zhang and Z. D. Zhang, *Phys. Rev. B*, 2005, **72**, 024411.

25 B. S. Wang, C. C. Li, J. C. Lin, S. Lin, P. Tong, X. B. Zhu, B. C. Zhao, W. J. Lu, Z. R. Yang, W. H. Song, J. M. Dai and Y. P. Sun, *Appl. Phys. Lett.*, 2010, **97**, 142505.

26 L. Ding, C. Wang, L. H. Chu, J. Yan, Y. Y. Na, Q. Z. Huang and X. L. Chen, *Appl. Phys. Lett.*, 2011, **99**, 251905.

27 K. Takenaka, A. Ozawa, T. Shibayama, N. Kaneko, T. Oe and C. Urano, *Appl. Phys. Lett.*, 2011, **98**, 022103.

28 T. Oe, C. Urano, N. Kaneko, M. Hadano and K. Takenaka, *Appl. Phys. Lett.*, 2013, **103**, 173518.

29 K. Asano, K. Koyama and K. Takenaka, *Appl. Phys. Lett.*, 2008, **92**, 161909.

30 A. L. Patterson, *Phys. Rev.*, 1939, **56**, 978-982.

31 D. Fruchart and E. F. Bertaut, *J. Phys. Soc. Jpn.*, 1978, **44**, 781.

32 B. S. Wang, P. Tong, Y. P. Sun, X. B. Zhu, X. Luo, G. Li, W. H. Song, Z. R. Yang and J. M. Dai, *J. Appl. Phys.*, 2009, **105**, 083907.

33 J. D. Livingston, *J. Appl. Phys.*, 1981, **52**, 2544-2548.

34 J. Nogues and I. K. Schuller, *J. Magn. Magn. Mater.*, 1999, **192**, 203-232.

35 J. Nogués, J. Sort, V. Langlais, V. Skumryev, S. Suriñach, J. S. Muñoz and M. D. Baró, *Phys. Rep.,* 2005, **422**, 65-117.

36 G. K. Rane, U. Welzel, S. R. Meka and E. J. Mittemeijer, *Acta Mater.*, 2013, **61**, 4524-4533.

37 K. Kamishima, T. Goto, T. Sasaki, T. Kanomata and T. Inami, *J. Phys. Soc. Jpn.,*2002, **71**, 922-926.

Figure captions:

Fig. 1 X-ray diffraction patterns at room temperature for $GaCMn_3$ subjected to ball milling of 0 hour (BM-0h) to 40 hours (BM-40h). The diffraction peaks are indexed with *Pm-3m* symmetry. Inset shows the refined lattice constant (a_0) as a function of milling time.

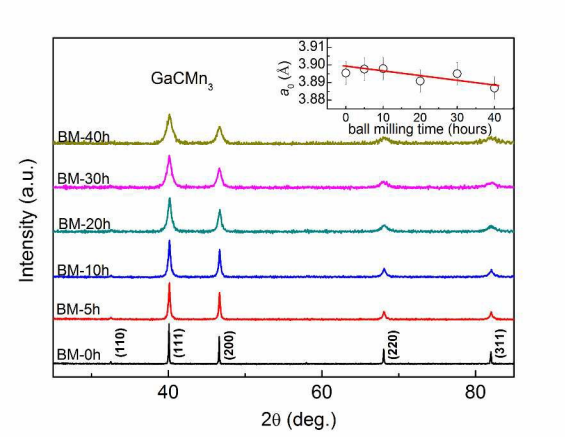

Fig. 2. FE-SEM images for nanocrystalline $GaCMn_3$ subjected to various milling intensities.

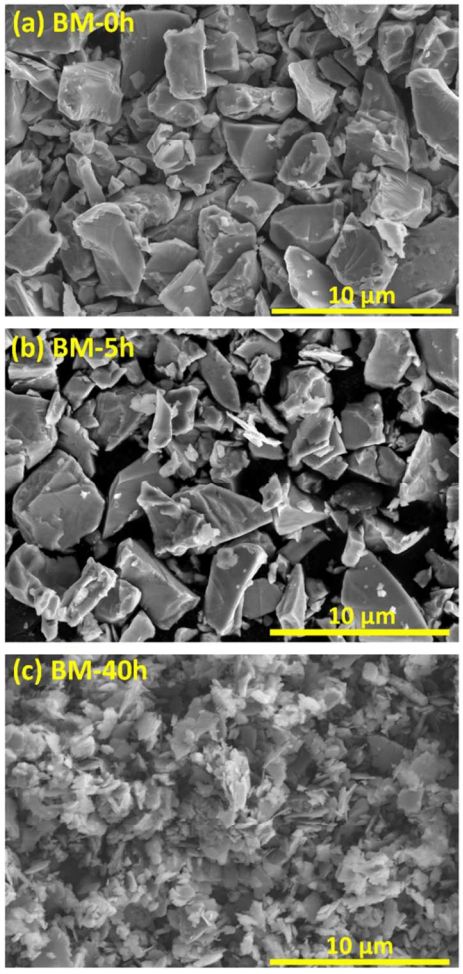

Fig. 3 (a) Temperature dependence of magnetization, M(T), measured at 100 Oe under zero-field-cooling mode for bulk and nanocrystalline $GaCMn_3$ samples with the average crystallite size varying from 45 *nm* to 9 *nm*. **(b)** The differential M(T), dM(T)/dT, for all samples. The characteristic temperatures, T_C, T_I and T_N were marked for the bulk sample. **(c)** The evolutions of magnetic transition temperatures, T_C, T_N and T_I as a function of average crystallite size (<D>). The verticle dotted line indicates the critical crystallite size of 15 nm (see text for details).

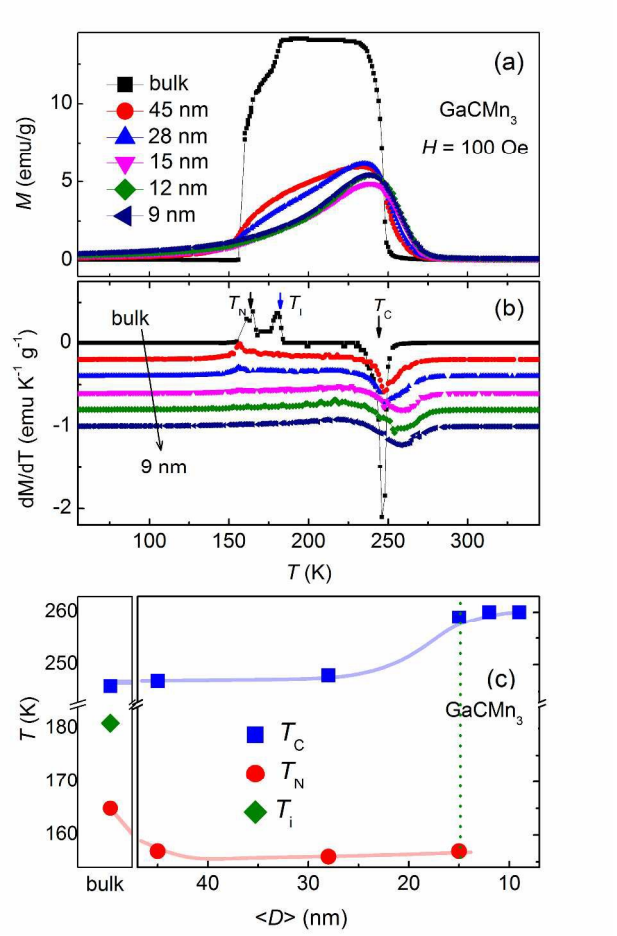

Fig. 4 (a) Field dependent magnetization, *M*(H), measured up to ± 45 kOe for $GaCMn_3$ with various average crystallite sizes (<*D*>). **(b)** The coercive field (H_C) and magnetization at 45 kOe (M_{45kOe}) as a function of <*D*>. The verticle dotted line indicates the critical crystallite size of 15 *nm* (see text for details).

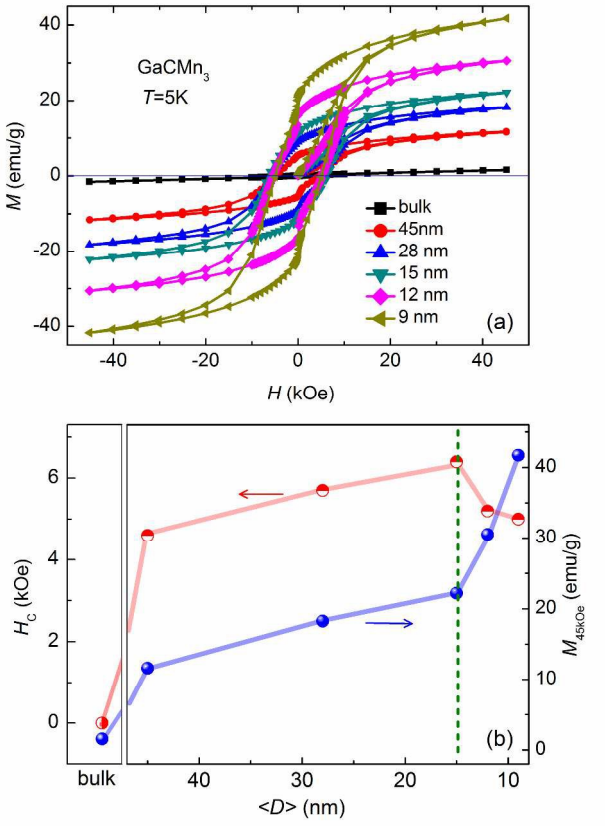

Fig. 5 (a) Field dependent magnetization, M(H), at various temperatures for nanocrystalline $GaCMn_3$ with an average crystallite size of <D> = 15 *nm*. **(b)** The coercive field (H_C) and magnetization at 45 kOe (M_{45kOe}) as a function of temperature.

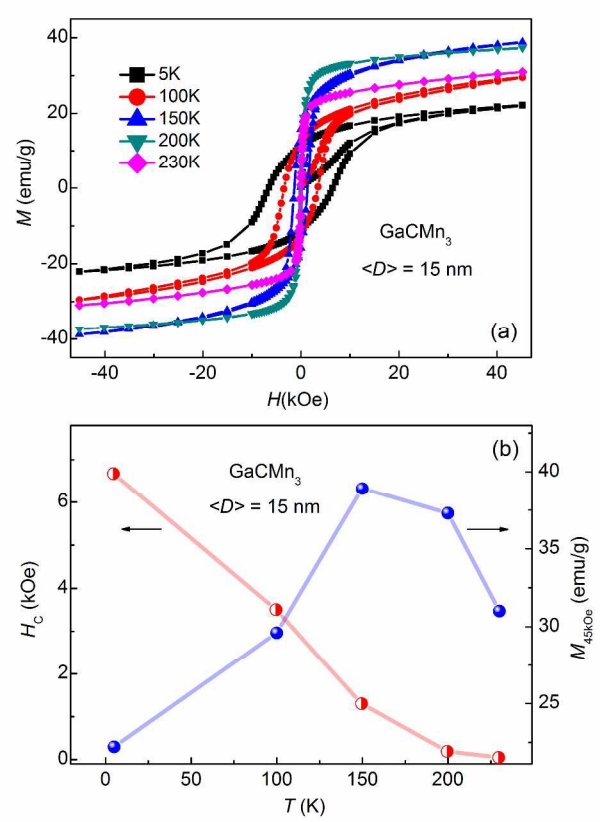

Fig. 6 (a) Temperature dependence of magnetization, M(T), measured at 100 Oe under zero-field-cooling mode for $GaNMn_3$ samples with various average crystallite sizes. **(b)** The differential M(T), dM(T)/dT, for all samples. **(c)** The antiferromagneti-paramagnetic transition temperature (T_N) as a function of average crystallite size (<D>). **(d)** Field dependent magnetization, M(H), measured up to ± 45 kOe at 5 K.